Published in final edited form as:
Dev Cell. 2010 December 14; 19(6): 845–857. doi:10.1016/j.devcel.2010.11.004.

mTORC2 REGULATES NEUTROPHIL CHEMOTAXIS IN A cAMP- AND RhoA-DEPENDENT FASHION

Lunhua Liu[1], **Satarupa Das**[1], **Wolfgang Losert**[1,2], and **Carole A. Parent**[1,*]

[1] Laboratory of Cellular and Molecular Biology, Center for Cancer Research, NCI, NIH, Bethesda, MD 20892

[2] Department of Physics, University of Maryland, College Park, MD 20742

SUMMARY

We studied the role of the target of rapamycin complex 2 (mTORC2) during neutrophil chemotaxis, a process that is mediated through the polarization of actin and myosin filament networks. We show that inhibition of mTORC2 activity, achieved via knock down (KD) of Rictor, severely inhibits neutrophil polarization and directed migration induced by chemoattractants, independently of Akt. Rictor KD also abolishes the ability of chemoattractants to induce cAMP production, a process mediated through the activation of the adenylyl cyclase 9 (AC9). Cells with either reduced or higher AC9 levels also exhibit specific and severe tail retraction defects that are mediated through RhoA. We further show that cAMP is excluded from extending pseudopods and remains restricted to the cell body of migrating neutrophils. We propose that the mTORC2-dependent regulation of MyoII occurs through a cAMP/RhoA signaling axis, independently of actin reorganization during neutrophil chemotaxis.

Keywords

neutrophils; chemotaxis; cAMP; target of rapamycin

INTRODUCTION

Chemotaxis is a process by which cells orient themselves and move up a chemical gradient. It is important in a variety of physiological and pathological events including nerve growth, angiogenesis, wound healing, metastatic invasion, and leukocyte trafficking. Neutrophil chemotaxis is induced by chemoattractants that signal through pertussis toxin sensitive Gi-coupled as well as G12/13-coupled receptors (Wang, 2009). Binding of chemoattractants to their receptors triggers the dissociation of the heterotrimeric G proteins into α- and βγ-subunits. The βγ-subunits act as the main transducers of chemotactic signals by activating several downstream effectors, including Ras, PI3K, and phospholipase C, which ultimately lead to cell polarization and migration (Bagorda et al., 2006).

*Corresponding Author: Carole A. Parent, Laboratory of Cellular and Molecular Biology, National Cancer Institute, National Institutes of Health, 37 Convent Drive, Bldg.37/Rm2066, Bethesda MD 20892-4256, Tel: 301-435-3701 FAX: 301-496-8479, parentc@mail.nih.gov.

The target of rapamycin (TOR) is an evolutionarily conserved serine/threonine kinase that integrates signals from growth factors, nutrients, and stress to regulate multiple processes, including mRNA translation, cell-cycle progression, autophagy, and cell survival (Bhaskar and Hay, 2007). In mammals, mTOR is the component of two distinct multiprotein complexes, mTOR complex 1 (mTORC1) and 2 (mTORC2). mTORC1 is sensitive to rapamycin and contains mTOR and three associated proteins: raptor, PRAS40, and mLST8. mTORC1 controls protein synthesis and cell growth by phosphorylating the translation regulator eIF-4E-binding protein 1 (4E-BP1) and the protein kinase AGC member S6 kinase 1 (S6K1) (Sengupta et al., 2010). mTORC2 is insensitive to rapamycin and is composed of mTOR, Rictor, mLST8, mSin1, and Protor1 and 2 (Cybulski and Hall, 2009). mTORC2 modulates cell survival in response to growth factors by phosphorylating Akt, serum/glucocorticoid regulated kinase 1 (SGK1), and protein kinase Cα (PKCα). mTORC2 has also been found to regulate actin cytoskeleton organization and cell migration in NIH 3T3, LN-18, U373, Rh30, and Hela cells (Gulati et al., 2009; Jacinto et al., 2004; Liu et al., 2006). However, the mechanism by which this takes place has not been elucidated. In the social amoebae *Dictyostelium discoideum*, the role of TORC2 in chemotaxis has been extensively studied. Cells lacking LST8, Rip3 (the mSin1 homologue), or Pianissimo (the Rictor homologue) all exhibit cell polarity and chemotaxis defects (Chen et al., 1997; Lee et al., 2005; Lee et al., 1999). Interestingly, it was recently demonstrated that these events are regulated by the TORC2-mediated, PI3K-independent PKBR1 phosphorylation, which occurs specifically at the leading edge of chemotaxing cells (Kamimura et al., 2008).

In *Dictyostelium*, TORC2 is also essential for the chemoattractant-mediated activation of the adenylyl cyclase ACA, which converts ATP into cAMP (Chen et al., 1997; Lee et al., 2005; Lee et al., 1999). In this system, Gβγ independently activates PI3K and TORC2 (Comer et al., 2005; Lee et al., 2005) and both signals are required for ACA activation (Chen et al., 1997). While PI3K acts through the pleckstrin homology (PH) domain-containing protein cytosolic regulator of adenylyl cyclase (CRAC) (Comer et al., 2005; Insall et al., 1994), the TORC2-mediated ACA activation is regulated through Akt and PKBR1, a homologue of Akt (Cai et al., 2010). Once synthesized, cAMP remains inside cells and regulates chemotaxis by inhibiting lateral pseudopod formation in a PKA-dependent fashion (Stepanovic et al., 2005). cAMP is also secreted and acts as the main chemoattractant in *Dictyostelium* by binding to specific G protein-coupled receptors (Garcia and Parent, 2008). In neutrophils, it is well established that the addition of chemoattractants triggers a transient increase in intracellular cAMP levels (Ali et al., 1998; Spisani et al., 1996; Suzuki et al., 1996). However, a clear correlation between cAMP levels and chemotaxis remains to be established (Elferink and VanUffelen, 1996; Harvath et al., 1991; Spisani et al., 1996). We have shown that chemoattractants give rise to a robust and transient activation of adenylyl cyclase in neutrophils that is sensitive to pertussis toxin treatment, but not to inhibition of PI3K activity (Mahadeo et al., 2007). We also established that adenylyl cyclase (AC) 3, 4, 7, and 9 are expressed in human neutrophils and suggested that AC9 is the predominant functional AC isoform in these cells (Mahadeo et al., 2007). However, the molecular components linking Gi-coupled chemoattractant receptors to ACs remain to be identified.

In this report, we set out to elucidate the role of mTORC2 during neutrophil chemotaxis. We show that cells lacking mTORC2 activity exhibit strong chemotaxis defects and loss of cell polarity. Remarkably, we establish that this phenotype is due to a loss of polarized actin assembly and myosin II (MyoII) regulation, the latter occurring in a cAMP- and RhoA-dependent fashion. Together, these findings provide novel insight into the fundamental role of cAMP in chemoattractant-mediated processes and present mechanistic information on how mTORC2 regulates cytoskeletal elements during migration.

RESULTS

Rictor is required for neutrophil chemotaxis

We first assessed if components of mTORC2 are present in neutrophils and PLB-985 cells - a pluripotent hematopoietic cell line that can be differentiated into neutrophil-like cells (Tucker et al., 1987). We found that both mTOR and Rictor are expressed in neutrophils and PLB-985 cells, and that their expression is dramatically enhanced upon differentiation of PLB-985 cells into neutrophil-like cells (Fig. 1A and data not shown). We screened potential active small hairpin RNAs (shRNA) that specifically target the human Rictor mRNA and used shRNA 1 and 2 to create stable PLB-985 Rictor shRNA cells that retained 20 +/− 8 % and 21 +/− 7 % Rictor protein levels, compared to control non-specific (NS) shRNA expressing cells (Fig. 1B). We differentiated PLB-985 cells into neutrophil-like cells by incubating them with 1.3% DMSO for 6 days (differentiated PLB-985 cells are referred as WT) and found that Rictor knock down (KD) does not alter the ability of PLB-985 cells to be differentiated into neutrophil-like cells (Fig. S1A). To determine the effect of Rictor KD on mTORC2 function, we measured the ability of N-formylmethionyl-leucyl-phenylalanine (fMLP), a strong chemoattractant secreted by bacteria (Marasco et al., 1984), to phosphorylate Akt (Bagorda et al., 2006) in differentiated NS and Rictor shRNA cells. While fMLP induced a robust phosphorylation of Akt at Ser473 in NS shRNA cells, a site known to be phosphorylated by mTORC2 (Sarbassov et al., 2005), in Rictor shRNA cells P-Akt Ser473 was dramatically inhibited (Fig. S1B). Yet, fMLP still induced a robust phosphorylation on Thr308 of Akt (a site known to be phosphorylated by PDK1 (Alessi et al., 1997)) in both cell lines (Fig. S1B), showing that Ser473 phosphorylation is not a major regulator of Ser308 phosphorylation in neutrophils as reported by other (Frias et al., 2006; Guertin et al., 2006; Jacinto et al., 2006; Shiota et al., 2006).

We compared the chemotactic ability of WT, NS shRNA, and Rictor shRNA cells under various conditions. We first used the under-agarose assay to assess the ability of large populations of cells to respond to chemotactic cues. We observed that, in contrast to WT and NS shRNA cells, Rictor shRNA cells do not migrate out of the loading wells toward a well containing an optimal amount of fMLP (Fig. 1C & S1C; similar results were obtained with LTB_4 (data not shown)). To gain further insight into this, we examined the behavior of the various cells using the Taxiscan chemotaxis chamber, where cells are exposed to linear gradients of chemoattractants (Nitta et al., 2007). Under these conditions, the Rictor shRNA cells again exhibited dramatic chemotaxis defects. While the NS shRNA cells traversed the well efficiently, the Rictor shRNA cells essentially remained in place (Fig. 1D & S3E, Movie S1). Similar findings were obtained using the micropipette assay. In these experiments, we mixed WT with NS shRNA or Rictor shRNA cells and exposed them to a micropipette containing 1 μM fMLP. The behavior of the shRNA expressing cells, which were easily identified because they also expressed GFP, was therefore directly comparable to WT cells. The NS shRNA cells rapidly polarized and migrated to the tip of the micropipette much like the WT cells (Fig. 1E & Movie S2). The Rictor shRNA cells were also able to sense the presence of chemoattractants as they quickly adhered to the plate (Movie S2). However, in contrast to NS shRNA cells, they did not appear to effectively polarize. Indeed, these cells showed a uniform F-actin accumulation throughout their periphery upon fMLP addition (Fig. 1F & S1D). Yet, the levels and kinetics of actin polymerization were identical in NS and Rictor shRNA cells (Fig. 1G) and the uropod marker, CD43, also remained polarized in Rictor KD cells (Fig. S1E). It therefore appears that the defect in polarity is not resulting from weaker signals to actin assembly or to polar-cap formation defects, although Rictor KD cells do not show distinct uropods.

Since both mTORC1 and mTORC2 have been shown to regulate cell migration, we used rapamycin treatment to assess the role of mTORC1 during neutrophil chemotaxis.

Neutrophils isolated from fresh human blood were treated with rapamycin for 30 min or 24 hrs. The specificity of these treatments on mTORC1 and mTORC2 was determined by assessing mTORC1-mediated p70S6K Thr389 phosphorylation as well as mTORC2-mediated Akt Ser473 phosphorylation. As previously shown in Hela and PC3 cells (Sarbassov et al., 2006), while short-term rapamycin treatment gave rise to a specific inhibition of p70S6K phosphorylation, long-term treatment clearly inhibited both mTORC1 and mTORC2 (Fig. S2A). Using transwell assays, we measured both fMLP- and GM-CSF-mediated chemotaxis. As previously shown (Gomez-Cambronero, 2003), we found that short-term rapamycin treatment strongly inhibited GM-CSF-mediated neutrophil chemotaxis (Fig. S2B). Yet, the same treatment did not significantly modify fMLP-mediated chemotaxis (Fig. S2B). In contrast, long-term rapamycin treatment of neutrophils, which did not alter cell viability, dramatically blocked fMLP-induced neutrophil chemotaxis (Fig. S2B). Similar findings were obtained using the Taxiscan assay (Fig. 2A & S2D, Movie S3) as well as the micropipette assay (data not shown). Together, these findings show that mTORC2 specifically regulates G protein coupled receptor-mediated neutrophil chemotaxis.

Rictor regulates chemotaxis and chemoattractant-induced cAMP accumulation in an Akt-independent and PKC-dependent fashion

As Akt is one of the downstream effectors of mTORC2, we assessed the role of Akt during neutrophil chemotaxis. We used the Akt inhibitor VIII, a highly specific Akt inhibitor that maintains Akt in its PH domain-in conformation and dramatically impairs Akt activity (Calleja et al., 2009). We found that Akt inhibition completely abolished the fMLP-induced Akt Ser473 and Akt Thr308 phosphorylation in both primary blood neutrophils and in differentiated PLB-985 cells (Fig. S2C; data not shown). Using the under-agarose assay, we found that Akt inhibition markedly, but not completely, inhibited neutrophil and differentiated PLB-985 chemotaxis (Fig. 2B; data not shown). However, no significant difference between untreated and treated neutrophil or differentiated PLB-985 cells was measured using the Taxiscan assay (Fig. 2C & S2D, Movie S3; data not shown). As Akt inhibition does not mimic the strong chemotaxis defect of the Rictor shRNA cells, we conclude that Akt does not mediate the mTORC2 effects on chemotaxis in neutrophils. We envision that the effect of Akt inhibition on the under-agarose migration underscores a specific role for Akt during migration in restricted environments that could be partly dependent on mTORC2.

As mTORC2 has been reported to mediate its effects on the actin cytoskeleton via PKC (PKC) in yeast and mammalian cells (Loewith et al., 2002; Sarbassov et al., 2004), we next studied role of PKC in neutrophil chemotaxis. Neutrophils isolated from human blood were incubated with GO6976, a specific conventional PKC (cPKC) inhibitor (Qatsha et al., 1993), and processed for chemotaxis assays. Using the under-agarose assay, we found that cPKC inhibition completely inhibited chemotaxis to fMLP (Fig. 2B). Remarkably, when chemotaxis was assessed using the Taxiscan assay, we observed that cPKC inhibited neutrophils could migrate directionally, but in contrast to untreated controls, the back of the inhibited cells remained strongly attached to the surface and did not retract, leading to cells with long, extended tails (Fig. 2D & Movie S3). We conclude that while cPKC inhibition leads to strong chemotaxis defects, cPKC does not completely mediate the effects of mTORC2 on neutrophil chemotaxis.

As TORC2 is essential for chemoattractant-mediated ACA activation in *Dictyostelium*, we next studied the role of mTORC2 in regulating chemoattractant-mediated cAMP synthesis. While WT, NS shRNA, and Rictor shRNA cells exhibited similar basal cAMP levels, the fMLP- and LTB_4-mediated increases in cAMP levels were specifically absent in Rictor shRNA cells (Fig. 2E & S2E; data not shown). Yet, Akt inhibition did not alter fMLP- or LTB_4-mediated cAMP accumulations in primary blood neutrophils and differentiated

PLB-985 cells (Fig. 2F & S2F) again establishing that Akt does not mediate the mTORC2 effects on neutrophil function. On the other hand, cPKC inhibition dramatically inhibited fMLP- and LTB_4-mediated cAMP production (Fig. 2F & S2F).

Knockdown of AC9 expression inhibits chemoattractant-induced cAMP production and chemotaxis

To gain insight into the importance of chemoattractant-induced cAMP increases in mediating the effects of mTORC2, we studied the role of cAMP during neutrophil chemotaxis. As pharmacological interventions aimed at inhibiting cAMP signaling are often toxic and non-specific, we set out to generate cells that are specifically devoid of chemoattractant-mediated cAMP increases. From our previous knowledge of adenylyl cyclases in neutrophils, we proposed that AC9 is the predominant isoform in these cells (Mahadeo et al., 2007). We therefore generated cells with reduced AC9 expression and assessed their ability to synthesize cAMP in response to chemoattractant stimulation. We screened potential active small hairpin RNAs (shRNA) that specifically target the human AC9 mRNA and identified two sequences, shRNA 1 and 2, that give rise to a dramatic decrease in AC9 mRNA levels (Fig. 3A). Similar to Rictor KD, we found that AC9 KD did not alter the ability of PLB-985 cells to be differentiated into neutrophil-like cells (Fig. S3A). We next measured intracellular cAMP levels in response to chemoattractant addition. We found that cells expressing AC9 shRNA had much lower intracellular cAMP basal levels that were barely increased after fMLP or LTB_4 addition (Fig. 3B, S3B, & S3C). Together, these findings establish that chemoattractant-mediated cAMP synthesis is mediated through the activation of AC9 in neutrophils.

To assess the role of chemoattractant-mediated cAMP fluxes during neutrophil chemotaxis, we compared the chemotactic ability of WT, NS shRNA, and AC9 shRNA cells. We observed that, in contrast to WT and NS shRNA cells, AC9 shRNA cells did not migrate efficiently out of the loading wells toward a well containing fMLP (Fig. 3C & S3D; similar results were obtained with LTB_4). Taxiscan analyses revealed that, like NS shRNA cells, AC9 shRNA cells appear to be able to sense the chemoattactant gradient as they properly oriented and polarized. However, in contrast to NS shRNA cells and similarly to cPKC inhibited cells, the back of AC9 shRNA cells remained strongly attached to the cover slip and did not effectively retract (Fig. 3D & S3E, Movie S1). In accordance with this, the AC9 shRNA cells barely moved across half of the chemotactic chamber by the end of the movie. This behavior was readily observed when 0.01, 0.1, or 1 μM fMLP was used, showing that the chemotactic defect was not secondary to a chemoattractant sensitivity issue (data not shown). The inability of the AC9 shRNA cells to move when placed in a chemoattractant gradient was also obvious using the micropipette assay. In contrast to the Rictor shRNA cells, the AC9 shRNA cells were able to polarize toward the tip of the micropipette, as evidenced by the presence of active membrane ruffling in the direction of the gradient. Yet, AC9 shRNA cells did not effectively migrate and basically remained stationary (Fig. 3E & Movie S4).

Exogenous expression of AC9 inhibits chemoattractant-induced cAMP production and chemotaxis

To gain more insight into the role of AC9 during neutrophil chemotaxis, we generated PLB-985 cells exogenously expressing AC9-Venus. As negative and positive controls, we constructed PLB-985 cells exogenously expressing Venus or AC3-eGFP, which is also expressed in neutrophils (Mahadeo et al., 2007) (Fig. S4A & B). We first studied the cellular distribution of AC3-eGFP and AC9-Venus in chemotaxing cells and found that both enzymes remain uniformly distributed on the plasma membrane in response to chemotactic signals (Fig. 4A) – an observation that is confirmed by looking at a 3D reconstruction from

confocal z stacks of AC9-Venus cells (data not shown). As anticipated, we measured significantly higher basal intracellular cAMP levels in both AC3-eGFP and AC9-Venus expressing cells compared to Venus and WT cells, showing that both enzymes are over-expressed and functional (Fig. 4B). Interestingly, while we found that fMLP stimulation resulted in a significant increase in cAMP levels in AC3-eGFP cells, cAMP production remained flat in AC9-Venus cells (Fig. 4B). We reason that, similarly to *Dictyostelium* cells over-expressing ACA (Pitt et al., 1992), in AC9-Venus cells, upstream regulators are limited and cannot activate the greater number of AC9-Venus molecules present. In contrast, in AC3-eGFP cells, WT levels of endogenous AC9 are present and chemotactic signals are normally transduced. Indeed, when we silenced AC9 expression in AC3-eGFP cells, fMLP-mediated cAMP accumulation was lost (Fig. 4C & S4C). Furthermore, as expected, these cells exhibited back retraction and chemotaxis defects similar to AC9 KD cells (data not shown).

We next examined the chemotactic properties of AC9-Venus cells. Using the under-agarose assay, we found that, like Venus cells, AC3-eGFP cells are able to sense the chemoattractant gradient and migrate efficiently toward fMLP or LTB_4. In contrast, most of the AC9-Venus cells stayed in the loading well with only a few cells migrating out (Fig. 4D & S4D). The chemotaxis defect of AC9-Venus cells was more carefully examined using the micropipette assay. While Venus and AC3-eGFP cells displayed similar normal chemotactic behaviors, the AC9-Venus cells developed very long tails as they tried to migrate up the chemoattractant gradient (data not shown, Fig. 4E & Movie S5). Therefore, similar to the KD of AC9 and cPKC inhibition, AC9-Venus expression did not affect the ability of cells to sense the chemoattractant gradient and polarize. Rather, altering AC9 levels affects the ability of cells to retract their back during chemotaxis. These behaviors were also readily evident when we used interference reflection microscopy (IRM) to quantify the overall adhesion pattern of both AC3-eGFP and AC9-Venus cells in response to chemoattractant stimulation (Fig. 4F & Movie S6). We found that AC9-Venus cells extended long footprints at their back following chemoattractant stimulation when compared to either Venus or AC3-eGFP cells. We conclude that both the exogenous expression and the KD of AC9 in PLB-985 cells lead to the loss of chemoattractant-mediated cAMP production and to significant chemotactic defects.

cAMP is excluded from extending pseudopods in randomly migrating and chemotaxing neutrophils

The back and side retraction defects observed in both AC9 shRNA and AC9-Venus cells prompted us to study the cellular distribution of cAMP in chemotaxing neutrophils. To this end we used a previously characterized cAMP FRET sensor, which harbors the PKA regulatory subunit cAMP binding domain (B domain) flanked by eYFP and eCFP (Bagorda et al., 2009). At low cAMP levels, the probe remains in a close state and the FRET response is maximal. However, in the presence of cAMP, a conformational change occurs and the FRET response is lost. NS shRNA and AC9 shRNA cells stably expressing the cAMP probe were differentiated, exposed to uniform fMLP stimulus and the FRET responses were measured. Cells expressed a uniform cytoplasmic distribution of the probe and comparable levels of the eCFP and eYFP signals (Fig. S5A). Figure 5A depicts images of the basal FRET signal observed in both cell lines. As expected from our biochemical measurements (Fig. 3B), AC9 shRNA cells show a significantly higher basal FRET signal compared to NS shRNA cells (Fig. 5B). Upon the addition of a uniform fMLP stimulus we measured a sharp and robust decrease in FRET efficiency (corresponding to higher cAMP levels) specifically in the cell body of NS cells – the FRET efficiency at the front of cells did not change upon fMLP addition and remained high throughout the time course of the experiment (Fig. 5C, Movie S7, the FRET signal remained unchanged in the cell body of cells treated with buffer

as depicted in Fig. S5B). Furthermore, no change in FRET efficiency was observed in either AC9 shRNA cells or in NS shRNA cells expressing a mutated version of the probe lacking the ability to bind cAMP (Bagorda et al., 2009) (Fig. 5C). Together, these findings show that the probe recognizes AC9-specific changes in cAMP concentrations that occur specifically within the cell body of stimulated cells.

To gain more insight into the dynamics nature of the cellular pool of cAMP, we exposed NS shRNA cells expressing the cAMP probe to a micropipette filled with fMLP and assessed the FRET response in actively chemotaxing cells. We observed a higher FRET signal exclusively at the extending pseudopods that persisted as the cells migrated (Fig. 5D & Movie S7). Yet, as we found following uniform chemoattractant stimulation, we measured a decrease in the FRET signal (corresponding to increases in cAMP levels) in the cell body as the cells moved toward the tip of the micropipette. Figure 5E presents a representative graph of the average FRET intensity along the migration axis of a cell at successive times as the cell is chemotaxing. It shows the extent by which the FRET intensity peaks at the extending pseudopod of migrating cells in a region several μm wide. This establishes that cAMP levels are lowest at the front of cells, where extensive actin remodeling takes place. In addition, while the FRET signal remained highest at the front of cells and lowest in the cell body, we observed a dynamic change in FRET levels at the back of chemotaxing cells, where the signal intermittently went up and down during chemotaxis (Fig. 5E & Movie S7). Taken together, these findings show that cAMP levels are regulated in a spatio-temporal fashion during chemotaxis. Whereas we measure lower levels in extending pseudopods, the back of cells exhibit dynamic cAMP variations as cells migrate toward the micropipette.

AC9 regulates RhoA activity and phosphorylated Myosin II levels

As MyoII activity regulates tail retraction/adhesion (Ridley et al., 2003), we next assessed MyoII activity in AC9-Venus cells by visualizing the cellular distribution of phosphorylated myosin regulatory light chain (P-MLC) following chemoattractant stimulation. As previously described, we found P-MLC predominantly enriched at the posterior cortex and back in polarized Venus and AC3-eGFP cells (Fig. 6A) (Wong et al., 2007). In contrast, in AC9-Venus and AC9 KD cells, the distribution of P-MLC dramatically extended to the front of cells and the level of P-MLC was much stronger than in Venus or AC3-eGFP cells (Fig. 6A). Similarly, Rictor shRNA cells, which are devoid of fMLP-mediated increase in cAMP levels and exhibit strong polarity defects, displayed a weakly polarized bright P-MLC staining at their periphery compared to NS shRNA cells (Fig. 6A). To provide more quantitative data, P-MLC levels were assessed by Western analyses following a uniform stimulation with fMLP. As shown by immunofluorescence, we found that cells that did not show an increase production of cAMP following fMLP addition (AC9-Venus, AC9 KD, and Rictor KD) also showed a dramatic and consistent increase in the level of P-MLC (Fig. 6B & S6A).

As Rho-associated kinase (ROCK) regulates MLC phosphorylation (Amano et al., 1996; Kimura et al., 1996), we next asked if ROCK inhibition could suppress the strong chemotaxis phenotype of the AC9 shRNA cells. For these experiments we mixed WT cells with AC9 shRNA cells, which are labeled with GFP, subjected them to a micropipette containing fMLP and allowed the cells to migrate directionally. We added DMSO, which had no effect, followed by 1 μM of the ROCK inhibitor Y-27632 (Uehata et al., 1997) (Fig. S6B & Movie S8). This low concentration of Y-27632 induced the formation of longer tails on the WT cells, but did not otherwise inhibit their directed migration. On the other hand, Y-27632 treatment suppressed the migration defect of the AC9 shRNA cells and allowed them to efficiently migrate toward the micropipette tip, much like WT cells. We conclude that the migration defects associated with alterations in AC9 activity is mediated by

increased MyoII phosphorylation levels, which leads to problems in back retraction and efficient migration.

Since the small GTP binding protein RhoA regulates back retraction by activating ROCK (Riento and Ridley, 2003), we next measured RhoA activation. We found that for both WT and Venus cells, fMLP exposure gave rise to a drop in RhoA activity after 1 min, followed by an enhancement in activity at the 5 min time point (Fig. 6C & S6C). Interestingly, these findings do not match RhoA-GTP levels measured in suspended cells, which typically show low basal activity followed by an increase in RhoA activity (Shi et al., 2009; Xu et al., 2005). We reason that this is related to the fact that we perform our assays on cells that are plated on fibronectin-coated surfaces as we wish to mimic signals that occur during migration. In contrast to what we measured in WT and Venus cells, AC9 shRNA and Rictor shRNA cells exhibited high constitutive RhoA activity that was not increased after fMLP addition. Furthermore, AC9-Venus cells showed a sustained RhoA activity as early as 1 min after stimulation (Fig. 6C & S6C). Interestingly, these RhoA activity dynamics are inversely correlated with the cAMP dynamics we measured in WT, AC9-Venus, AC9 shRNA, and Rictor shRNA cells. In WT cells, a peak in cAMP levels occurs early after fMLP addition when RhoA activity is low (Fig. 3B). In contrast, in AC9-Venus and AC9 or Rictor shRNA cells, where fMLP-mediated increases in cAMP levels are modest (AC9-Venus, Fig. 4B) or absent (AC9 shRNA, Fig. 3B; Rictor shRNA, Fig. 2E), we observed more sustained RhoA activity. These findings show that the loss of chemoattractant-mediated cAMP accumulations in AC9-Venus, AC9 shRNA, and Rictor shRNA cells leads to constitutive RhoA-GTP levels, giving rise to high ROCK activity and P-MLC levels in these cells. Together, these effects lead to enhanced back activity and inefficient migration.

DISCUSSION

mTORC2 has been shown to be involved in regulating the actin cytoskeleton in various systems (Cybulski and Hall, 2009). Consistent with findings in *Dictyostelium* (Chen et al., 1997; Lee et al., 2005), we now establish that mTORC2 is a key regulator of neutrophil polarity and chemotaxis. We show that mTORC2 profoundly regulates the ability of neutrophils to polarize F-actin and P-MyoII and to migrate directionally as well as to produce cAMP in response to chemoattractant stimulation. As we find that AC9 KD cells specifically exhibit P-MyoII defects, we envision that mTORC2 mediates its effects on cell polarity by regulating both the actin and MyoII filament assembly independently. We provide evidence that mTORC2 mediates its effects on MyoII assembly through a cAMP- and RhoA-dependent pathway. The mechanism by which mTORC2 regulates the actin cytoskeleton remains to be determined (Cybulski and Hall, 2009). We do show that the defect in polarity does not result from weaker signals to F-actin assembly. Rather, Rictor seems to regulate where F-actin is enriched. As shown in *Dictyostelium* (Lee et al., 2005), we do not envision that this is regulated through altered PIP_3 distribution. In *Dictyostelium*, the effect of TORC2 on chemotaxis has been shown to occur through PKBR1, a homologue of Akt that is myristoylated and persistently localized at the plasma membrane, independently of PI3K (Kamimura et al., 2008). We now show that Akt inhibition does not alter neutrophil chemotaxis to a micropipette or in the Taxiscan chamber, confirming results obtained with neutrophils isolated from *Akt1*$^{-/-}$ mice (Di Lorenzo et al., 2009). It therefore appears that mTORC2 mediates its effect on the actin cytoskeleton independently of Akt in neutrophils. Importantly, our findings also confirm previous reports showing that uropod formation is dependent on the RhoA/ROCK/MyoII pathway (Lee et al., 2004; Rossy et al., 2009), as Rictor KD cells do not display uropods.

From our findings, we propose that chemoattractant-mediated mTORC2-dependent, transient cAMP accumulations are required to control back contraction and relaxation

phases that occur during chemotaxis through phosphorylation and dephosphorylation cycles of MyoII. We propose that MyoII phosphorylation/dephosphorylation phases are regulated by two antagonistic pathways that act downstream of chemoattractant receptor activation (Fig. 7). The activating pathway has been proposed to be mediated via coupling to G12/13, which activates RhoA through PDZ-RhoAGEF (Wong et al., 2007;Xu et al., 2003). We now provide evidence that the inhibitory pathway is controlled via coupling to Gi, through AC9, in an mTORC2-dependent fashion. We envision that cAMP, through PKA activation, provides antagonistic signals to the RhoA/MyoII signaling pathway by phosphorylating RhoA, as previously reported (Ellerbroek et al., 2003;Lang et al., 1996). The inhibitory effects of PKA may also be mediated through phosphorylation of MLCK, which inhibits its activity (Howe, 2004). In addition, PKA has also been shown to negatively regulate at least two RhoAGEFs: RhoAGEF Lfc (Meiri et al., 2009) and AKAP-Lbc (Diviani et al., 2006). It will be interesting to determine if either of these also impact RhoA activity in neutrophils. Remarkably, although MyoII activity is stimulated by phosphorylation of MLC at Ser19, the stability of MyoII filaments has been shown to be more significantly regulated by MLC dephosphorylation at Thr18 and Ser19 (Ikebe et al., 1988) and the dephosphorylation step is required for rapid filament assembly through rapid disassembly of preexisting filaments (Watanabe et al., 2007). We envision that as cells are chemotaxing up chemoattractant gradients, they experience increase receptor activation that trigger activating and inhibitory signals leading to the cycling of MyoII phosphorylation and dephosphorylation and optimal migration.

The relationship between intracellular cAMP levels and neutrophil chemotaxis has been controversial, with studies reporting either stimulatory or inhibitory effects (Elferink and VanUffelen, 1996; Harvath et al., 1991; Spisani et al., 1996). One reason for such discrepancy is the use of pharmacological activators and inhibitors of adenylyl cyclases, phosphodiesterases, or PKA, which can exhibit non-specific effects. In addition, the robust unregulated activation of these enzymes can lead to non-physiological effects. Indeed, Jones and colleagues have argued that spatially restricted PKA activity is at play during neutrophil chemotaxis (Jones and Sharief, 2005). Our FRET analyses show that chemoattractant-mediated cAMP fluxes occur specifically in the cell body and back of neutrophils, where cAMP is poised to regulate RhoA. Remarkably, we also establish that cAMP is specifically excluded from extending pseudopods of randomly moving and chemotaxing cells. While the mechanism underlying this remains to be determined, we envision that a spatially activated pool of phosphodiesterase is active in pseudopods and maintains low cAMP levels. In any case, the spatial restriction of cAMP to the cell body of neutrophils provides a pool where cAMP can specifically act on effectors that regulate retraction and contraction at the sides and back of polarized cells. Indeed, traction forces have been shown to occur largely at the side and rear of migrating neutrophils (Smith et al., 2007). We now suggest that the spatio-temporal cAMP changes elicited by chemoattractants tightly regulate these forces by acting on RhoA and MyoII phosphorylation.

The synthesis of intracellular cAMP is tightly regulated by adenylyl cyclases. Mammalian genomes harbor nine distinct G protein-coupled adenylyl cyclases (AC1-AC9), composed of two sets of six transmembrane domains followed by conserved cytosolic catalytic loops (Sunahara and Taussig, 2002). While all transmembrane ACs are stimulated by Gαs, only AC1, AC5, AC6 and AC8 are inhibited by Gαi. Interestingly, all four ACs isoforms expressed in neutrophils (AC3, AC4, AC7, and AC9) are insensitive to Gαi inhibition (Hacker et al., 1998; Mahadeo et al., 2007; Sunahara and Taussig, 2002). Combined with our previous findings (Mahadeo et al., 2007), we now establish that chemoattractant-mediated cAMP accumulations in neutrophils are dependent on AC9 through Gi-coupled signals. Unlike Gs-coupled receptors, which activate AC by the direct interaction of GTP-Gαs with AC, we reason that the released Gβγ subunits from Gi-coupled receptors, in

concert with cytosolic components, activate AC. In *Dictyostelium*, chemoattractant receptors activate ACA in a Gβγ-dependent fashion and require input from the PI3K-dependent cytosolic regulator of adenylyl cyclase (CRAC) and TORC2 (Chen et al., 1997; Insall et al., 1994; Lee et al., 2005). While input from PI3K is not required for AC9 activation in neutrophils (Mahadeo et al., 2007), we now establish that chemoattractant-mediated cAMP accumulations are dependent on mTORC2, therefore highlighting the strong evolutionary conservation of signaling cascades between these two systems. The mechanism by which mTORC2 activates AC9 remains to be determined. We do show that the chemoattractant-mediated activation of AC9 depends on cPKC but not Akt. As cPKC has been proposed to be controlled by mTORC2 (Sarbassov et al., 2004), we predict that mTORC2 regulates AC9 activity through PKC. As many of the components of the AC activation cascade are membrane bound and TORC2 activity has been found to be spatially activated at the leading edge of *Dictyostelium* cells (Kamimura et al., 2008), we envision that mTORC2 translocates to the plasma membrane where it is poised to activate cPKC and AC9 upon chemoattractant addition in neutrophils.

EXPERIMENTAL PROCEDURES

Additional information is found in the Supplemental Information Section.

Cell lines

HEK293T cells (ATCC) and Phoenix cells (Orbigen Inc, San Diego, CA) were maintained on 100-mm plate in DMEM media containing 10% fetal bovine serum, 25 mM HEPES, 100 units/ml penicillin and 100 mg/ml streptomycin at 37°C, 5% CO_2. For virus packaging, 80% confluence of cells were used for transient transfection with lipofectamine methods. PLB-985 cells were maintained in an undifferentiated state in RPMI1640 media containing 10% fetal bovine serum, 25 mM HEPES, 100 units/ml penicillin and 100 mg/ml streptomycin at 37°C, 5% CO_2. Cells were differentiated at a density of 4.5×10^5 cells/ml for 6 days in 1.3% DMSO RPMI1640 complete media and the status of differentiation was monitored by CD11b staining.

Construct and Transfection of PLB-985 Cells

A retroviral approach was used to create a stable population of PLB-985 cells expressing Venus, AC3-eGFP and AC9-Venus. See Supplemental Information for more details.

Chemotaxis Assay

1. Micropipette chemotaxis assay: Differentiated cells were plated on chambered cover slides coated with 0.2% gelatin, and a chemotactic gradient was generated using the Eppendorf microinjector with Fentotips (Eppendorf, Germany) loaded with 1 μM fMLP.
2. Under-agarose assay: Chemotaxis of a large population of cells was observed with the under-agarose assay, as described previously (Comer et al., 2005). 5×10^5 differentiated cells were resuspended in 5 μl mHBSS and plated into the outer wells. The middle well was filled with 500 nM fMLP or 500 nM LTB_4 in mHBSS, and the gradient was allowed to establish for 10 min before plating cells. After the cells were allowed to chemotaxis for ~4 hrs, the wells were carefully overlayed with phosphate buffer and visualized on a Leica DM IL stereoscope. Each assay was performed in triplicate, and the results are representative of at least three independent experiments on different days. Quantification was performed by comparing the pixel intensity in a selected area outside the well (see yellow box in

Fig. 1D) where the cells were loaded in buffer and chemoattractant conditions using Image J. The pixel intensity in the buffer condition was normalized to 1.

3. EZ-Taxiscan chemotaxis assay: The EZ-Taxiscan chamber (Effector Cell Institute, Tokyo, Japan) was assembled as described by the manufacturer. Cell migration was recorded every 15 sec for 30 min at 37°C in a humidified environmental chamber. Coverslips and chips used in the chamber were coated with 1% BSA at RT for 1 hr. All glass coverslips were ultrasonicated and washed before use. Cell migration analysis was conducted with MATLAB software. Single cells were tracked over time using an algorithm for finding multiple objects in images (Crocker and Grier, 1996). The average image was subtracted to avoid tracking dead cells or other stationary features. Cell tracks were subsequently used to compute chemotaxis index (CI) and speed for each tracked cell in each time-step, as well as the average CI and average speed for an experiment. Each image shows a representative section of the final frame in the experiment, plus the locations of all cells identified and tracked in the section in all frames. The color indicates time: going from red to blue as time evolves.

RhoA-GTP Pull-Down Assay

The pull-down assay for RhoA-GTP was performed as described in (Wojciak-Stothard et al., 2007) on cells plated on fibronectin-coated 12-wells tissue-culture plates following 1 μM fMLP addition. See Supplemental Information for more details.

Live cell FRET imaging and analysis

A series of time-lapse images were collected as previously described (Bagorda et al., 2009). Briefly, to measure FRET, images were acquired for each set of measurements: (1) YFP fluorescence (514 nm excitation, 530 nm LP emission filter); (2) CFP fluorescence (458 nm excitation, 475–505 nm BP emission filter) and (3) FRET (458 nm, 530 nm LP emission filter). In order to obtain a corrected FRET image, we acquired reference images from CFP-YFP expressing cells which do not FRET (using the same set of acquisition parameters) and processed using pFRET software (CircuSoft Instrumentation LLC, Hockessin, DE). The FRET efficiency images were used to obtain an average of FRET efficiency values, which were further normalized to the average of the images preceding fMLP stimulation as a reference value set to 100%.

Supplementary Material

Refer to Web version on PubMed Central for supplementary material.

Acknowledgments

We thank Drs. Daniel Storm for providing the cDNA encoding AC3 and AC9, Henry Bourne for providing the PLB-985 cells, and Paul Randazzo for providing the Rhotekin-sepharose beads and for helpful advice. We also wish to thank the Parent laboratory members for excellent discussions and suggestions and for valuable input on the manuscript. A special thanks goes to Dr. Valarie Barr for her help with the microscopy. WL performed this work while on sabbatical at the LCMB, CCR. This research was supported by the Intramural Research Program of the Center for Cancer Research, NCI, National Institutes of Health.

References

Alessi DR, Deak M, Casamayor A, Caudwell FB, Morrice N, Norman DG, Gaffney P, Reese CB, MacDougall CN, Harbison D, et al. 3-Phosphoinositide-dependent protein kinase-1 (PDK1): structural and functional homology with the Drosophila DSTPK61 kinase. Curr Biol. 1997; 7:776–789. [PubMed: 9368760]

Ali H, Sozzani S, Fisher I, Barr AJ, Richardson RM, Haribabu B, Snyderman R. Differential regulation of formyl peptide and platelet-activating factor receptors. Role of phospholipase Cbeta3 phosphorylation by protein kinase A. J Biol Chem. 1998; 273:11012–11016. [PubMed: 9556582]

Amano M, Ito M, Kimura K, Fukata Y, Chihara K, Nakano T, Matsuura Y, Kaibuchi K. Phosphorylation and activation of myosin by Rho-associated kinase (Rho-kinase). J Biol Chem. 1996; 271:20246–20249. [PubMed: 8702756]

Bagorda A, Das S, Rericha EC, Chen D, Davidson J, Parent CA. Real-time measurements of cAMP production in live Dictyostelium cells. J Cell Sci. 2009; 122:3907–3914. [PubMed: 19808889]

Bagorda A, Mihaylov VA, Parent CA. Chemotaxis: moving forward and holding on to the past. Thromb Haemost. 2006; 95:12–21. [PubMed: 16543956]

Bhaskar PT, Hay N. The two TORCs and Akt. Dev Cell. 2007; 12:487–502. [PubMed: 17419990]

Cai H, Das S, Kamimura Y, Long Y, Parent CA, Devreotes PN. Ras-mediated activation of the TORC2-PKB pathway is critical for chemotaxis. J Cell Biol. 2010; 190:233–245. [PubMed: 20660630]

Calleja V, Laguerre M, Parker PJ, Larijani B. Role of a novel PH-kinase domain interface in PKB/Akt regulation: structural mechanism for allosteric inhibition. PLoS Biol. 2009; 7:e17. [PubMed: 19166270]

Chen MY, Long Y, Devreotes PN. A novel cytosolic regulator, Pianissimo, is required for chemoattractant receptor and G protien-mediated activation of the 12 transmembrane domain adenylyl cyclase in *Dictyostelium*. Genes and Development. 1997; 11:3218–3231. [PubMed: 9389653]

Comer FI, Lippincott CK, Masbad JJ, Parent CA. The PI3K-mediated activation of CRAC independently regulates adenylyl cyclase activation and chemotaxis. Curr Biol. 2005; 15:134–139. [PubMed: 15668169]

Crocker JC, Grier DG. Methods of digital video microscopy for colloidal studies. J Colloid Interface Sci. 1996; 179:298–310.

Cybulski N, Hall MN. TOR complex 2: a signaling pathway of its own. Trends Biochem Sci. 2009; 34:620–627. [PubMed: 19875293]

Di Lorenzo A, Fernandez-Hernando C, Cirino G, Sessa WC. Akt1 is critical for acute inflammation and histamine-mediated vascular leakage. Proc Natl Acad Sci U S A. 2009; 106:14552–14557. [PubMed: 19622728]

Diviani D, Baisamy L, Appert-Collin A. AKAP-Lbc: a molecular scaffold for the integration of cyclic AMP and Rho transduction pathways. Eur J Cell Biol. 2006; 85:603–610. [PubMed: 16460837]

Elferink JGR, VanUffelen BE. The role of cyclic nucleotides in neutrophil migration. Gen Pharmacol. 1996; 27:387–393. [PubMed: 8919662]

Ellerbroek SM, Wennerberg K, Burridge K. Serine phosphorylation negatively regulates RhoA in vivo. J Biol Chem. 2003; 278:19023–19031. [PubMed: 12654918]

Frias MA, Thoreen CC, Jaffe JD, Schroder W, Sculley T, Carr SA, Sabatini DM. mSin1 is necessary for Akt/PKB phosphorylation, and its isoforms define three distinct mTORC2s. Curr Biol. 2006; 16:1865–1870. [PubMed: 16919458]

Garcia GL, Parent CA. Signal relay during chemotaxis. J Microsc. 2008; 231:529–534. [PubMed: 18755009]

Gomez-Cambronero J. Rapamycin inhibits GM-CSF-induced neutrophil migration. FEBS Lett. 2003; 550:94–100. [PubMed: 12935893]

Guertin DA, Stevens DM, Thoreen CC, Burds AA, Kalaany NY, Moffat J, Brown M, Fitzgerald KJ, Sabatini DM. Ablation in mice of the mTORC components raptor, rictor, or mLST8 reveals that mTORC2 is required for signaling to Akt-FOXO and PKCalpha, but not S6K1. Dev Cell. 2006; 11:859–871. [PubMed: 17141160]

Gulati N, Karsy M, Albert L, Murali R, Jhanwar-Uniyal M. Involvement of mTORC1 and mTORC2 in regulation of glioblastoma multiforme growth and motility. International journal of oncology. 2009; 35:731–740. [PubMed: 19724909]

Hacker BM, Tomlinson JE, Wayman GA, Sultana R, Chan G, Villacres E, Disteche C, Storm DR. Cloning, chromosomal mapping, and regulatory properties of the human type 9 adenylyl cyclase (ADCY9). Genomics. 1998; 50:97–104. [PubMed: 9628827]

Harvath L, Robbins JD, Russell AA, Seamon KB. cAMP and human neutrophil chemotaxis. Elevation of cAMP differentially affects chemotactic responsiveness. J Immunol. 1991; 146:224–232. [PubMed: 1701793]

Howe AK. Regulation of actin-based cell migration by cAMP/PKA. Biochim Biophys Acta. 2004; 1692:159–174. [PubMed: 15246685]

Ikebe M, Inagaki M, Naka M, Hidaka H. Correlation of conformation and phosphorylation and dephosphorylation of smooth muscle myosin. J Biol Chem. 1988; 263:10698–10704. [PubMed: 2839501]

Insall R, Kuspa A, Lilly PJ, Shaulsky G, Levin LR, Loomis WF, Devreotes PN. CRAC, a cytosolic protein containing a pleckstrin homology domain, is required for receptor and G protein-mediated activation of adenylyl cyclase in *Dictyostelium*. J Cell Biol. 1994; 126:1537–1545. [PubMed: 8089184]

Jacinto E, Facchinetti V, Liu D, Soto N, Wei S, Jung SY, Huang Q, Qin J, Su B. SIN1/MIP1 maintains rictor-mTOR complex integrity and regulates Akt phosphorylation and substrate specificity. Cell. 2006; 127:125–137. [PubMed: 16962653]

Jacinto E, Loewith R, Schmidt A, Lin S, Ruegg MA, Hall A, Hall MN. Mammalian TOR complex 2 controls the actin cytoskeleton and is rapamycin insensitive. Nature cell biology. 2004; 6:1122–1128.

Jones SL, Sharief Y. Asymmetrical protein kinase A activity establishes neutrophil cytoskeletal polarity and enables chemotaxis. J Leukoc Biol. 2005; 78:248–258. [PubMed: 15817703]

Kamimura Y, Xiong Y, Iglesias PA, Hoeller O, Bolourani P, Devreotes PN. PIP3-independent activation of TorC2 and PKB at the cell's leading edge mediates chemotaxis. Curr Biol. 2008; 18:1034–1043. [PubMed: 18635356]

Kimura K, Ito M, Amano M, Chihara K, Fukata Y, Nakafuku M, Yamamori B, Feng J, Nakano T, Okawa K, et al. Regulation of myosin phosphatase by Rho and Rho-associated kinase (Rho-kinase). Science. 1996; 273:245–248. [PubMed: 8662509]

Lang P, Gesbert F, Delespine-Carmagnat M, Stancou R, Pouchelet M, Bertoglio J. Protein kinase A phosphorylation of RhoA mediates the morphological and functional effects of cyclic AMP in cytotoxic lymphocytes. Embo J. 1996; 15:510–519. [PubMed: 8599934]

Lee JH, Katakai T, Hara T, Gonda H, Sugai M, Shimizu A. Roles of p-ERM and Rho-ROCK signaling in lymphocyte polarity and uropod formation. J Cell Biol. 2004; 167:327–337. [PubMed: 15504914]

Lee S, Comer FI, Sasaki A, McLeod IX, Duong Y, Okumura K, Yates JR 3rd, Parent CA, Firtel RA. TOR complex 2 integrates cell movement during chemotaxis and signal relay in Dictyostelium. Mol Biol Cell. 2005; 16:4572–4583. [PubMed: 16079174]

Lee S, Parent CA, Insall R, Firtel RA. A novel Ras-interacting protein required for chemotaxis and cyclic adenosine monophosphate signal relay in Dictyostelium. Mol Biol Cell. 1999; 10:2829–2845. [PubMed: 10473630]

Liu L, Li F, Cardelli JA, Martin KA, Blenis J, Huang S. Rapamycin inhibits cell motility by suppression of mTOR-mediated S6K1 and 4E-BP1 pathways. Oncogene. 2006; 25:7029–7040. [PubMed: 16715128]

Loewith R, Jacinto E, Wullschleger S, Lorberg A, Crespo JL, Bonenfant D, Oppliger W, Jenoe P, Hall MN. Two TOR complexes, only one of which is rapamycin sensitive, have distinct roles in cell growth control. Mol Cell. 2002; 10:457–468. [PubMed: 12408816]

Mahadeo DC, Janka-Junttila M, Smoot RL, Roselova P, Parent CA. A chemoattractant-mediated Gi-coupled pathway activates adenylyl cyclase in human neutrophils. Mol Biol Cell. 2007; 18:512–522. [PubMed: 17135293]

Marasco WA, Phan SH, Krutzsch H, Showell HJ, Feltner DE, Nairn R, Becker EL, Ward PA. Purification and identification of formyl-methionyl-leucyl-phenylalanine as the major peptide neutrophil chemotactic factor produced by Escherichia coli. J Biol Chem. 1984; 259:5430–5439. [PubMed: 6371005]

Meiri D, Greeve MA, Brunet A, Finan D, Wells CD, LaRose J, Rottapel R. Modulation of Rho guanine exchange factor Lfc activity by protein kinase A-mediated phosphorylation. Mol Cell Biol. 2009; 29:5963–5973. [PubMed: 19667072]

Nitta N, Tsuchiya T, Yamauchi A, Tamatani T, Kanegasaki S. Quantitative analysis of eosinophil chemotaxis tracked using a novel optical device -- TAXIScan. J Immunol Methods. 2007; 320:155–163. [PubMed: 17289072]

Pitt GS, Milona N, Borleis JA, Lin KC, Reed RR, Devreotes PN. Structurally distinct and stage-specific adenylyl cyclase genes play different roles in *Dictyostelium* development. Cell. 1992; 69:305–315. [PubMed: 1348970]

Qatsha KA, Rudolph C, Marme D, Schachtele C, May WS. Go 6976, a selective inhibitor of protein kinase C, is a potent antagonist of human immunodeficiency virus 1 induction from latent/low-level-producing reservoir cells in vitro. Proc Natl Acad Sci U S A. 1993; 90:4674–4678. [PubMed: 7685108]

Ridley AJ, Schwartz MA, Burridge K, Firtel RA, Ginsberg MH, Borisy G, Parsons JT, Horwitz AR. Cell migration: integrating signals from front to back. Science. 2003; 302:1704–1709. [PubMed: 14657486]

Riento K, Ridley AJ. Rocks: multifunctional kinases in cell behaviour. Nat Rev Mol Cell Biol. 2003; 4:446–456. [PubMed: 12778124]

Rossy J, Schlicht D, Engelhardt B, Niggli V. Flotillins interact with PSGL-1 in neutrophils and, upon stimulation, rapidly organize into membrane domains subsequently accumulating in the uropod. PLoS One. 2009; 4:e5403. [PubMed: 19404397]

Sarbassov DD, Ali SM, Kim DH, Guertin DA, Latek RR, Erdjument-Bromage H, Tempst P, Sabatini DM. Rictor, a novel binding partner of mTOR, defines a rapamycin-insensitive and raptor-independent pathway that regulates the cytoskeleton. Curr Biol. 2004; 14:1296–1302. [PubMed: 15268862]

Sarbassov DD, Ali SM, Sengupta S, Sheen JH, Hsu PP, Bagley AF, Markhard AL, Sabatini DM. Prolonged rapamycin treatment inhibits mTORC2 assembly and Akt/PKB. Mol Cell. 2006; 22:159–168. [PubMed: 16603397]

Sarbassov DD, Guertin DA, Ali SM, Sabatini DM. Phosphorylation and regulation of Akt/PKB by the rictor-mTOR complex. Science. 2005; 307:1098–1101. [PubMed: 15718470]

Sengupta S, Peterson TR, Sabatini DM. Regulation of the mTOR Complex 1 Pathway by Nutrients, Growth Factors, and Stress. Mol Cell. 2010; 40:310–322. [PubMed: 20965424]

Shi Y, Zhang J, Mullin M, Dong B, Alberts AS, Siminovitch KA. The mDial formin is required for neutrophil polarization, migration, and activation of the LARG/RhoA/ROCK signaling axis during chemotaxis. J Immunol. 2009; 182:3837–3845. [PubMed: 19265163]

Shiota C, Woo JT, Lindner J, Shelton KD, Magnuson MA. Multiallelic disruption of the rictor gene in mice reveals that mTOR complex 2 is essential for fetal growth and viability. Dev Cell. 2006; 11:583–589. [PubMed: 16962829]

Smith LA, Aranda-Espinoza H, Haun JB, Dembo M, Hammer DA. Neutrophil traction stresses are concentrated in the uropod during migration. Biophys J. 2007; 92:L58–60. [PubMed: 17218464]

Spisani S, Pareschi MC, Buzzi M, Colamussi ML, Biondi C, Traniello S, Pagani Zecchini G, Paglialunga Paradisi M, Torrini I, Ferretti ME. Effect of cyclic AMP level reduction on human neutrophil responses to formylated peptides. Cell Signal. 1996; 8:269–277. [PubMed: 8842527]

Stepanovic V, Wessels D, Daniels K, Loomis WF, Soll DR. Intracellular role of adenylyl cyclase in regulation of lateral pseudopod formation during Dictyostelium chemotaxis. Eukaryot Cell. 2005; 4:775–786. [PubMed: 15821137]

Sunahara RK, Taussig R. Isoforms of mammalian adenylyl cyclase: multiplicities of signaling. Mol Interv. 2002; 2:168–184. [PubMed: 14993377]

Suzuki T, Hazeki O, Hazeki K, Ui M, Katada T. Involvement of the beta gamma subunits of inhibitory GTP-binding protein in chemoattractant receptor-mediated potentiation of cyclic AMP formation in guinea pig neutrophils. Biochim Biophys Acta. 1996; 1313:72–78. [PubMed: 8781552]

Tucker KA, Lilly MB, Heck L Jr, Rado TA. Characterization of a new human diploid myeloid leukemia cell line (PLB-985) with granulocytic and monocytic differentiating capacity. Blood. 1987; 70:372–378. [PubMed: 3475136]

Uehata M, Ishizaki T, Satoh H, Ono T, Kawahara T, Morishita T, Tamakawa H, Yamagami K, Inui J, Maekawa M, et al. Calcium sensitization of smooth muscle mediated by a Rho-associated protein kinase in hypertension. Nature. 1997; 389:990–994. [PubMed: 9353125]

Wang F. The signaling mechanisms underlying cell polarity and chemotaxis. Cold Spring Harbor Perspect Biol. 2009; 1:a002980.

Watanabe T, Hosoya H, Yonemura S. Regulation of myosin II dynamics by phosphorylation and dephosphorylation of its light chain in epithelial cells. Mol Biol Cell. 2007; 18:605–616. [PubMed: 17151359]

Wojciak-Stothard B, Torondel B, Tsang LY, Fleming I, Fisslthaler B, Leiper JM, Vallance P. The ADMA/DDAH pathway is a critical regulator of endothelial cell motility. J Cell Sci. 2007; 120:929–942. [PubMed: 17327280]

Wong K, Van Keymeulen A, Bourne HR. PDZRhoGEF and myosin II localize RhoA activity to the back of polarizing neutrophil-like cells. J Cell Biol. 2007; 179:1141–1148. [PubMed: 18086913]

Xu J, Wang F, Van Keymeulen A, Herzmark P, Straight A, Kelly K, Takuwa Y, Sugimoto N, Mitchison T, Bourne HR. Divergent signals and cytoskeletal assemblies regulate self-organizing polarity in neutrophils. Cell. 2003; 114:201–214. [PubMed: 12887922]

Xu J, Wang F, Van Keymeulen A, Rentel M, Bourne HR. Neutrophil microtubules suppress polarity and enhance directional migration. Proc Natl Acad Sci U S A. 2005; 102:6884–6889. [PubMed: 15860582]

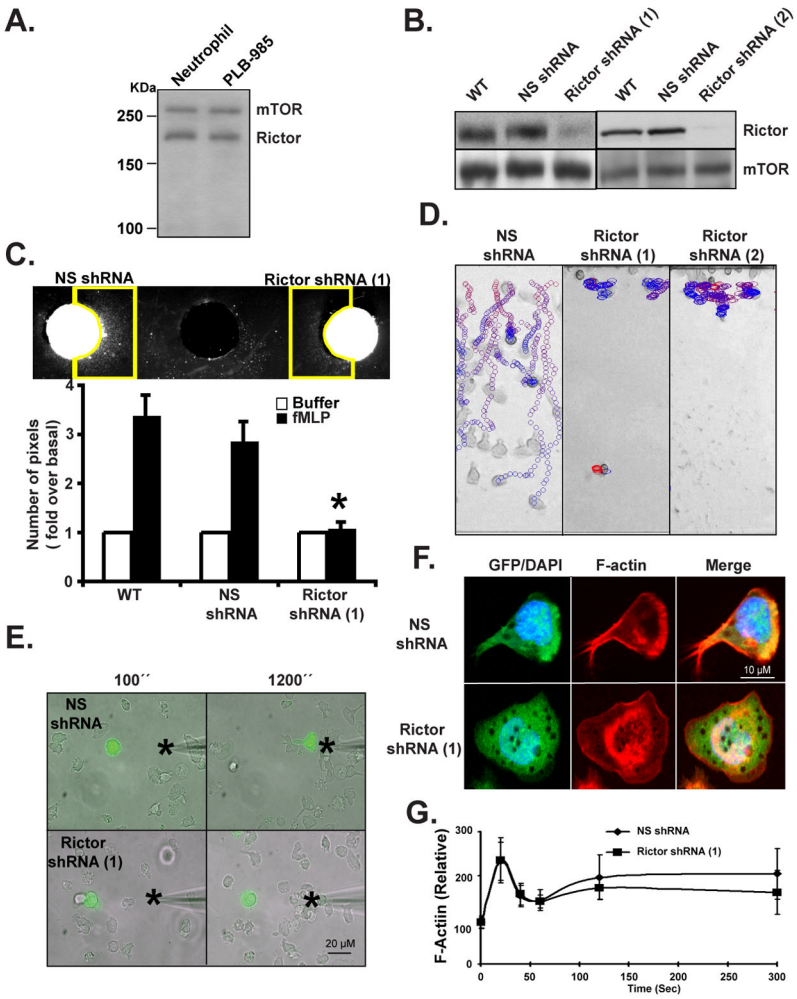

Figure 1. Rictor KD inhibits neutrophil chemotaxis

A. Rictor and mTOR are expressed in human blood neutrophils and PLB-985 cells. Cells were lysed and subjected to Western analyses using antibodies specific for Rictor and mTOR.

B. Rictor KD in PLB-985 cells. Cells were lysed and subjected to Western analyses using antibodies specific for Rictor, mTOR. Results are representative of three independent experiments. Also see Fig. S1A and S1B.

C. Under-agarose chemotaxis assay of Rictor shRNA cells. Central well contains 500 nM fMLP. Quantification was performed as described in the Experimental Procedures. Results represent the average +/− SD of three independent experiments. * indicates $p<0.01$ compared to the fMLP-stimulated WT group. Also see Fig. S1C.

D. EZ-Taxiscan chemotaxis towards fMLP of Rictor KD cells. The images show paths of individual cells migrating in a gradient of fMLP as circles (from red to blue with increasing time) overlaid onto the final frame. For clarity, only cells that moved in 10 consecutive frames are shown. However, all cells were included for quantification (see Fig. S3E). Data are representative of six independent experiments. Also see Movie S1.

E. Chemotaxis of Rictor KD cells to a point source of fMLP. Images depicting differentiated cells migrating to a micropipette containing 1 μM fMLP were captured every 10 secs. The star represents the position of the tip of the micropipette. Overlay of bright field and

fluorescent images are representative of three independent experiments are presented. Also see Movie S2.

F. Rictor shRNA cells show uniform F-actin accumulation after fMLP stimulation. Differentiated cells were stimulated with a uniform concentration of fMLP (1 μM) for 10 min and fixed. F-actin was detected by rhodamine-phalloidin staining. Results are representative of three independent experiments. Also see Fig. 1D.

G. Rictor shRNA cells show normal F-actin polymerization after fMLP stimulation. Differentiated cells were stimulated with a uniform concentration of fMLP (1 μM) and fixed at indicated time point. F-actin content was detected by rhodamine-phalloidin staining. Results represent the average +/− SD of three independent experiments. Also see Fig. 1E.

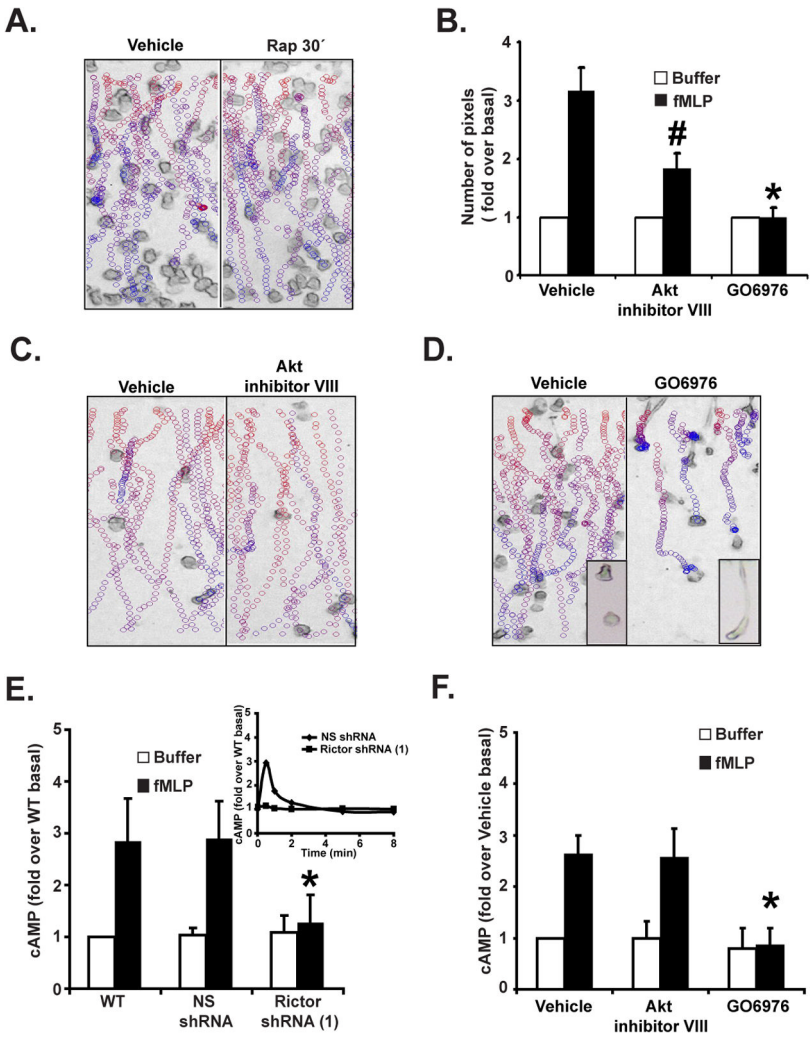

Figure 2. Rictor regulates chemotaxis and chemoattractant-induced cAMP accumulation in an Akt-independent and PKC-dependent fashion

A. EZ-Taxiscan chemotaxis towards fMLP of Rapamycin-treated human blood neutrophils. Neutrophils were treated with or without 100 nM Rapamycin for 30 min. Data are representative of three independent experiments. See legend Fig. 1D for details. Paths for 24 hrs treatment is not shown because no significant movement could be detected. Also see Fig. S2A, S2B, S2D, and Movie S3.

B. Under-agarose chemotaxis assay of Akt or cPKC-inhibited human blood neutrophils. Neutrophils were treated with or 10 μM Akt inhibitor VIII or 10 μM cPKC inhibitor GO6976 for 30 min. Central well contains 500 nM fMLP. Quantification was performed as described in Experimental Procedures. Results represent the average +/− SD of three independent experiments. # indicates $p<0.05$ compared to the vehicle fMLP group.

C. EZ-Taxiscan chemotaxis towards fMLP of Akt-inhibited human blood neutrophils. Neutrophils were treated with or without 10 μM Akt inhibitor VIII for 30 min. Data are representative of five independent experiments. See legend Fig. 1D for details. Also see Fig. S2D and Movie S3.

D. EZ-Taxiscan chemotaxis towards fMLP of cPKC-inhibited human blood neutrophils. Neutrophils were treated with or without 10 μM GO6976 for 30 min. Insert shows a higher

magnification image of the cells. Data are representative of five independent experiments. See legend Fig. 1D for details. Also see Fig. S2D and Movie S3.

E. Rictor KD inhibits fMLP-induced cAMP production. Differentiated cells were stimulated with 1 μM fMLP for 30 secs and intracellular cAMP levels were measured before and after chemoattractant addition. The inset shows the time-course measurement of intracellular cAMP levels. SEM values are presented from six independent experiments. * indicates $p<0.01$ compared to the fMLP-stimulated NS shRNA group. Also see Fig. S2E.

F. cPKC but not Akt regulates fMLP-induced cAMP production. Human blood neutrophils were treated with 10 μM Akt inhibitor VIII or 10 μM cPKC inhibitor GO6976 for 30 min. Intracellular cAMP levels were measured before and after chemoattractant addition. Results represent the average +/− SD of three independent experiments. * indicates $p<0.01$ compared to the fMLP-stimulated vehicle group. Also see Fig. S2F.

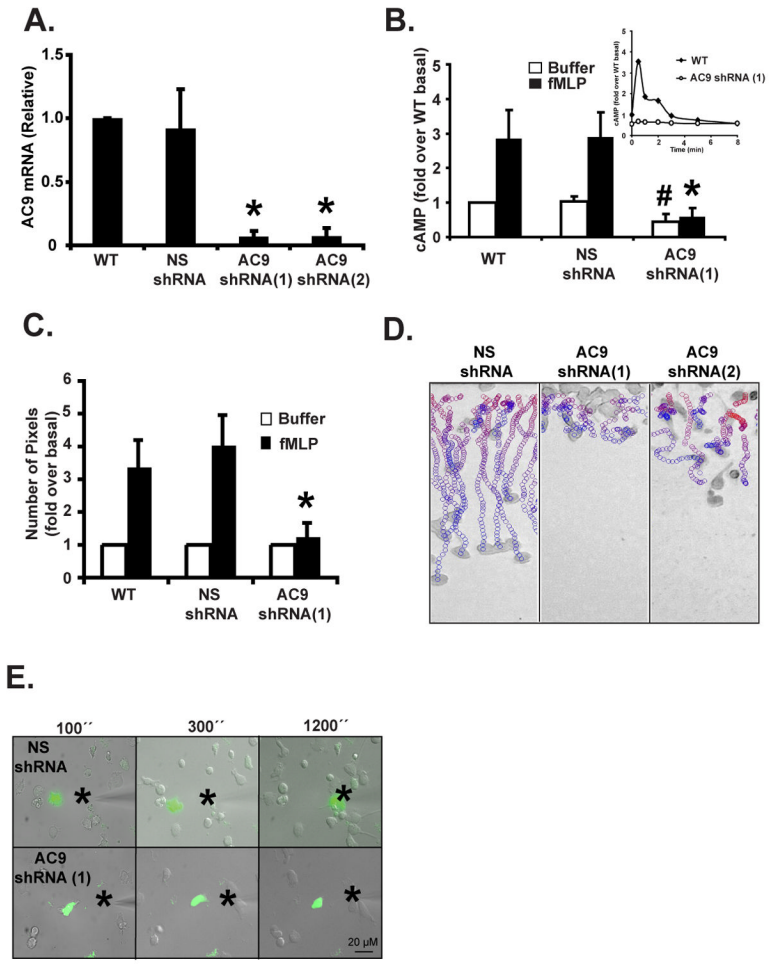

Figure 3. Chemoattractant-induced cAMP production is mediated by AC9 and is required for neutrophil chemotaxis

A. KD of AC9 expression in PLB-985 cells. Total RNA from cells was extracted and AC9 mRNA level were measured by Real-time RT PCR. Results represent the average +/− SD of three independent experiments. Also see Fig. S3A.

B. KD of AC9 expression inhibits chemoattractant-induced cAMP production. Intracellular cAMP levels were measured before and 30 secs after a 1 μM fMLP stimulation in differentiated cells. The inset shows the time-course measurement of intracellular cAMP levels. SEM values are presented from six independent experiments. # indicates $p<0.05$ compared to the buffer NS shRNA group; * indicates $p<0.01$ compared to the fMLP-stimulated NS shRNA group. Also see Fig. S3B & S3C.

C. Under-agarose chemotaxis assay of AC9 shRNA(1) cells. Central well contains 500 nM fMLP. Quantification was performed as described in Experimental Procedures. Results represent the average +/− SD of four independent experiments. * indicates $p<0.01$ compared to the fMLP-stimulated NS shRNA group. Also see Fig. S3D.

D. EZ-Taxiscan chemotaxis towards fMLP of AC9 KD cells. Data are representative of six independent experiments. See legend Fig. 1D for details. Also see Fig. S3E and Movie S1.

E. Chemotaxis of AC9 shRNA(1) cells to a point source of fMLP. Images depicting differentiated cells migrating to a micropipette containing 1 μM fMLP. The star represents the position of the tip of the micropipette. Overlay of bright field and fluorescent images are representative of three independent experiments are presented. Also see Movie S4.

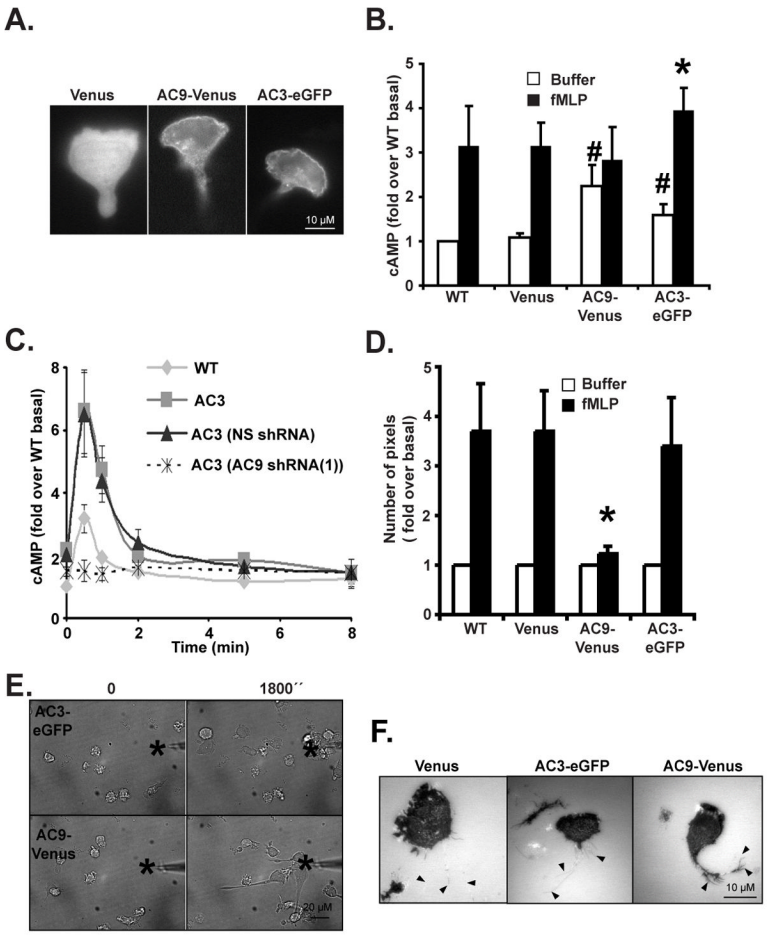

Figure 4. Exogenous expression of AC9 inhibits chemoattractant-induced cAMP production and chemotaxis

A. Fluorescent images depicting the sub-cellular distribution of Venus, AC3-eGFP or AC9-Venus in differentiated and migrating cells.

B. Over-expression of AC9 results in higher basal cAMP levels and inhibits chemoattractant-induced cAMP production. Differentiated cells were stimulated with 1 μM fMLP for 30 secs and intracellular cAMP levels were measured before and after chemoattractant addition. SEM values are presented from six independent experiments. # indicates $p<0.05$ compared to the buffer Venus group; * indicates $p<0.01$ compared to the fMLP-stimulated Venus group.

C. KD of AC9 inhibits chemoattractant-induced cAMP production in AC3-eGFP over-expressing cells. Differentiated cells were stimulated with 1 μM fMLP and intracellular cAMP levels were measured at indicated time point. The average +/− SD from three independent experiments. Also see Fig. S4C.

D. Under-agarose chemotaxis assay of AC9-Venus and AC3-eGFP cells. Central well contains 500 nM fMLP. Quantification was performed as described in Experimental Procedures. Results represent the averaged +/− SD of three independent experiments. * indicates $p<0.01$ compared to the fMLP-stimulated Venus group. Also see Fig. S4D.

E. AC9-Venus cells exhibit long tail during chemotaxis. Images depicting differentiated cells migrating to a micropipette containing 1 μM fMLP were captured every 10 secs. The star represents the position of the tip of the micropipette. Bright field images are representative of three independent experiments are presented. See also Movie S5.

F. AC9-Venus cells have stronger tail attachment. Differentiated cells were stimulated with 1 μM fMLP and IRM images were recorded every 10 secs. Black arrow heads represent the location of the tail from the phase images. Representative images are presented. Also see Movie S6.

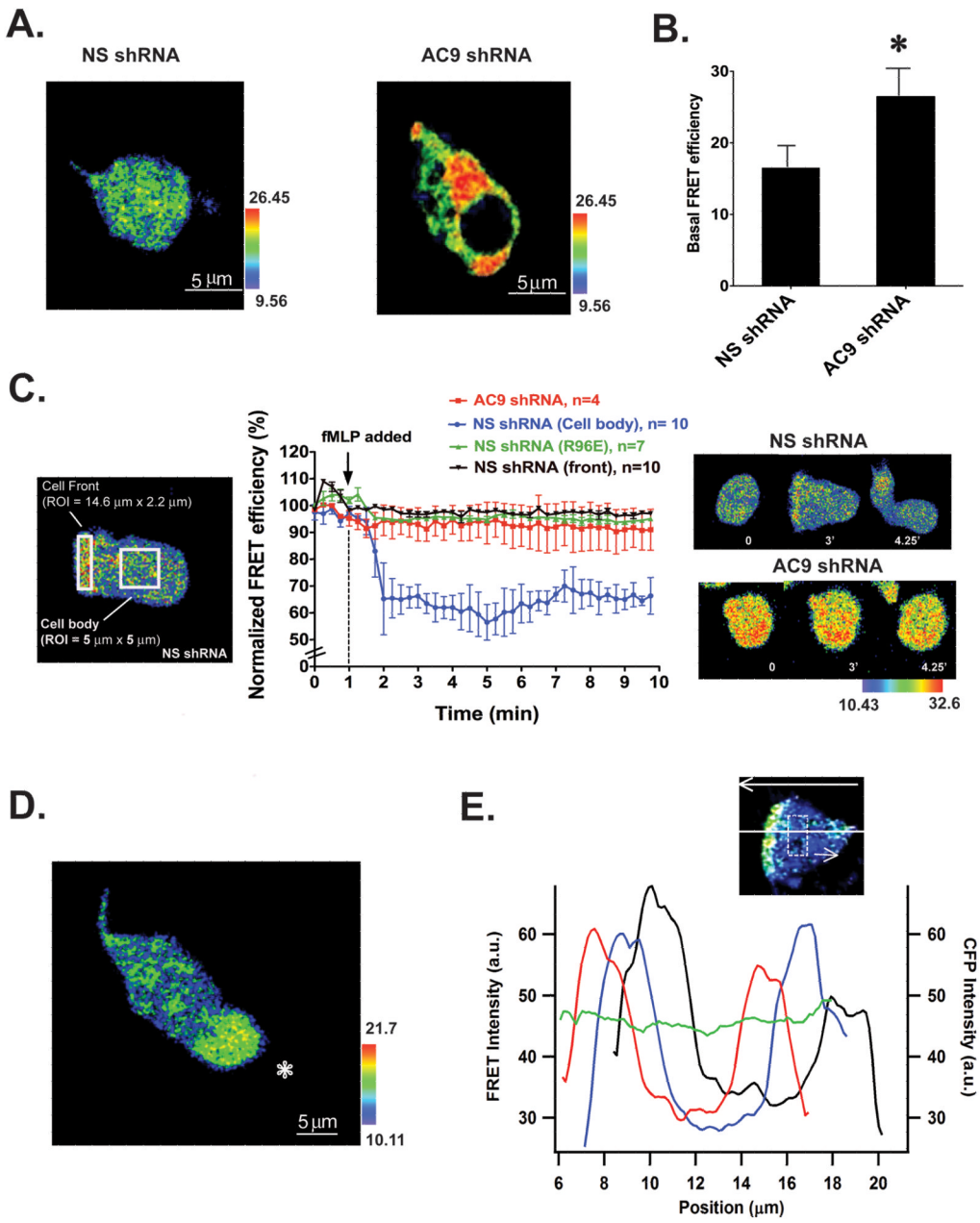

Figure 5. cAMP is excluded from extending pseudopods in randomly migrating and chemotaxing neutrophils

A. Basal FRET efficiency images represented in pseudo-color for differentiated NS shRNA and AC9 shRNA. Also see Fig. S5A. At low cAMP levels observed in AC9 KD cells, the probe remains in a close state and the FRET response is maximal. In the presence of cAMP, a conformational change occurs and the FRET response is lost.

B. Average basal FRET efficiency in differentiated NS shRNA and AC9 shRNA cells, n=8. * indicates $p<0.01$ compared to NS shRNA cells.

C. Time course of FRET efficiency following a uniform stimulation with 1 μM fMLP in NS shRNA and AC9 shRNA cells expressing the WT FRET sensor and in NS shRNA cells expressing a mutated FRET sensor (R96E). The left panel shows the area where the FRET efficiency was measured. The right panel depicts FRET efficiency images at different time

points for NS shRNA and AC9 shRNA cells expressing the WT FRET sensor. Also see Fig. S5B & Movie S7.

D. Differentiated NS shRNA cells were exposed to a micropipette containing 1 μM fMLP. The position of the micropipette is indicated by the star. The pseudocolor image was taken from a representative experiment and represents FRET efficiency. Also see Movie S7.

E. Graph depicting FRET intensities as a function of the position along the long axis of the cell for three consecutive time points acquired at 15 secs interval (depicted in red, blue and black lines). Each point is an average over a smoothing region 5.6 μm across the cell width and 2.1 μm along the long axis of the cell (dashed square indicates the size of the sliding smoothing region). The top arrow indicates the direction of cell migration. The green line depicts the intensity of CFP fluorescence across the cell.

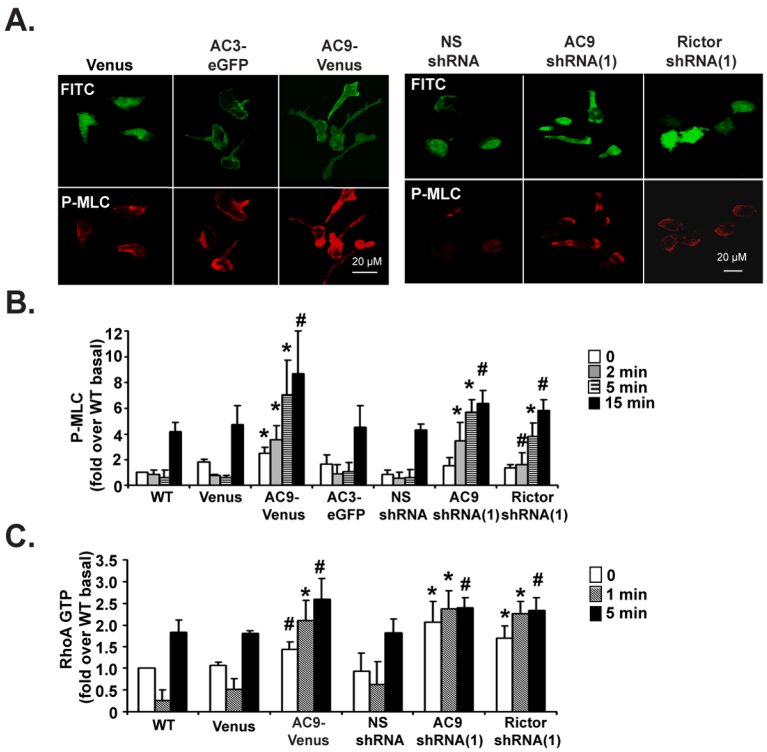

Figure 6. AC9 regulates RhoA activity and phosphorylated Myosin II levels

A. AC9-Venus and AC9 KD cells exhibit higher P-MLC staining. Differentiated cells were uniformly stimulated with 1 μM fMLP for 15 min and fixed. Representative dual images are presented.

B. AC9-Venus, AC9 shRNA, and Rictor shRNA cells show higher P-MLC levels. Differentiated cells were plated on fibronectin-coated plates for 10 min and uniformly stimulated with 1 μM fMLP. At specific time points, samples were subjected to Western analyses using an anti-P-MLC antibody. Quantification of three experiments is presented as the amount of P-MLC after fMLP stimulation relative to that of unstimulated cells (mean ± SD). The amount of P-MLC at each point was standardized by dividing its value with the value of total MLC of the same time point. Also see Fig. S6A. * indicates $p<0.01$ and # indicates $p<0.05$ compared to either Venus or NS shRNA cells.

C. AC9-Venus, AC9 shRNA, and Rictor shRNA cells show defects in RhoA-GTP activation. Differentiated cells were treated as in panel B. Quantification of three experiments is presented as the amount of RhoA-GTP after fMLP stimulation relative to that of WT unstimulated cells (mean ± SD). The amount of RhoA-GTP at each point was standardized by dividing its value with the value of total RhoA of the same time point. Also see Fig. S6C. * indicates $p<0.01$ and # indicates $p<0.05$ compared to either Venus or NS shRNA cells.

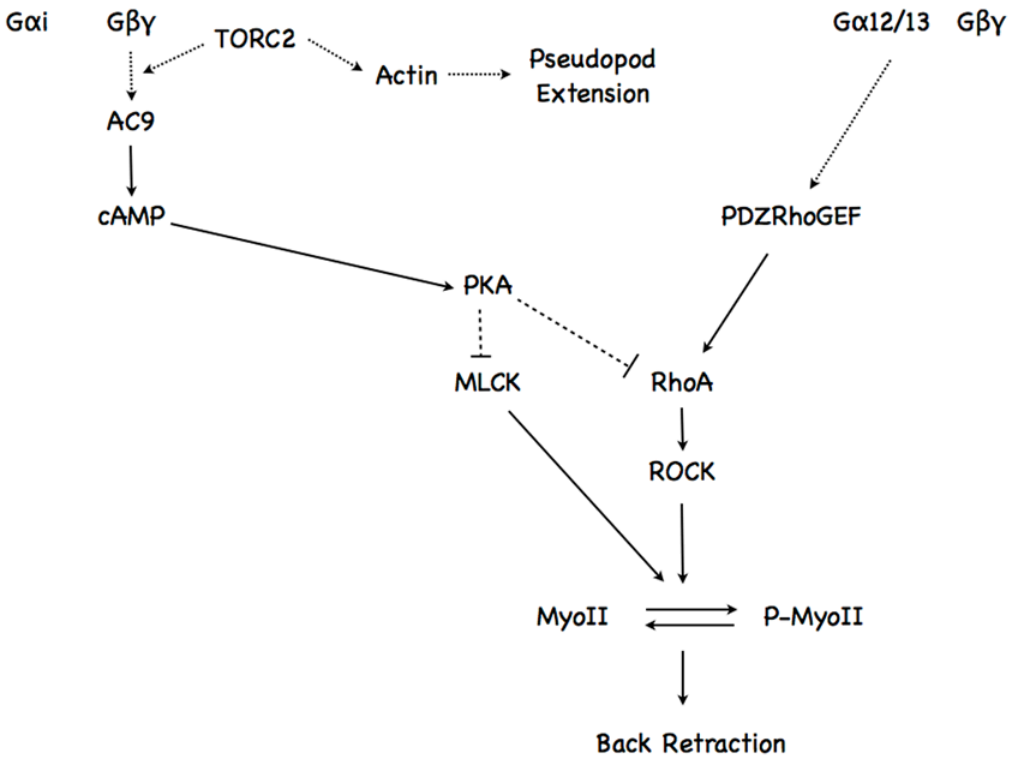

Figure 7. Schematic diagram depicting how chemoattractant-mediated increases in intracellular cAMP levels regulate neutrophil back retraction

See text for details.